



Research Article

Structural evolution of mechanically alloyed ODS steel powders during ball milling and subsequent annealing treatment

Emin Salur ^{a,*} 

^aSelcuk University, Faculty of Technology, Department of Metallurgical and Materials Engineering, Konya 42075, Turkey

ARTICLE INFO

Article history:

Received 18 February 2022

Accepted 29 May 2022

Published 15 August 2022

Keywords:

Annealing
Ball milling
Hardness
9Cr-ODS

ABSTRACT

In the present work, a novel 9Cr oxide-dispersion strengthened (ODS) steel powders with Y_2O_3 (0.5 wt%) dispersoids were synthesized by high planetary ball milling at different time intervals (2, 8, and 16 hours). The structural and crystallographical evolution of the produced powders during the ball milling and post-annealing treatment were evaluated by SEM, XRD, and micro-Vickers hardness analyses. The SEM results showed that the fine dispersions of powders were achieved with the extending milling time. When milling time was 8h, it was observed that the mean size of powders increased maximum level of 101 μm and then dramatically reduced to 5 μm at latest milling time (16h). The XRD data revealed that the crystallite size of ODS powders diminished gradually with increasing milling time. Plus, all reflection peaks of the Fe, Cr, W, Mo expanded and the diffraction peaks of the Y_2O_3 , W progressively disappeared with the increasing milling time. The hardness results revealed that the increasing milling time was beneficial for hardness improvement, due to dominant strain hardening mechanism and it developed from 160 to 334 Hv after 16h of milling protocol. To understand high temperatures characteristics such as grain growth, phase transformation, and hardness of produced powders, 16h milled powders subjected to post-annealing treatments at 700 °C and 900 °C for 1 h. When pure Fe and Cr peaks were observed in the non-annealed powders, no evident reflection peak of Y_2O_3 was observed. However, all pure Fe and Cr reflection peaks became narrower and Y_2O_3 reflection exhibited more sharper tendency with increased annealing temperatures, which resulted in increased grain growth and formation of Fe-based oxide structures.

1. Introduction

Oxide-dispersion strengthened (ODS) alloys contain very fine oxide particles and they are mainly used for structural applications for nuclear power plant constructions as piping and cladding tubes [1]. They are most important candidates for the fuel cladding materials owing to their extreme temperature strength, as well as their thermal stability at elevated temperatures and excellent resistance to corrosion [2-6]. The most diverse feature that differentiate ODS steels from other structural systems is that they have fine dispersoids comprising of several oxide based structures such as Al_2O_3 , Y_2O_3 , Ce_2O_3 or uniformly dispersed Y-Al-O, Y-Ti-O constituents at a high number density in the matrix [7, 8]. These nanoscale particles throughout the matrix, cause the secondary phase particles to prevent the movement of dislocations during deformation and resultant an increment of the density of dislocations in the material [9, 10].

ODS alloys are chiefly produced by the powder metallurgical ways, including ball milling/mechanical alloying of mixed powders with well dispersed oxide structures and followed consolidation and heating treatments [11]. The microstructural evolution and mechanical performance of ODS alloys greatly depends on process variables and chemical compositions. Generally, Y_2O_3 , Ce_2O_3 , La_2O_3 , MgO, ZrO_2 [12, 13] are added into ODS alloys as dispersed particles. Regarding the introduction of these dispersoids to the material system, which can generally harden the material, Y-based oxide structures are the foremost preferred ones due to its low solution ability in the base matrix, thermodynamically stable characteristics, and lattice divergence that favors their influence as dislocation propagation inhibiting dispersoids and their excellent irradiation stability performance [14].

Li et al. [7] examined that the influence of different types of nanoscales oxides (Y_2O_3 , Ce_2O_3 , La_2O_3) on the

* Corresponding author. Tel.: +90 332 223 3392.

E-mail addresses: esalur@selcuk.edu.tr (E. Salur)

ORCID: 0000-0003-0984-3496 (E. Salur)

DOI: [10.35860/iarej.1075508](https://doi.org/10.35860/iarej.1075508)

© 2022, The Author(s). This article is licensed under the CC BY-NC 4.0 International License (<https://creativecommons.org/licenses/by-nc/4.0/>).

microstructure changes and mechanical properties of produced 14Cr-ODS steels. As well as superb thermal stability of Y_2O_3 , they found that the Y_2O_3 added ODS alloys exhibit higher yield strength, have a lower particle size distribution and thus have a higher number density.

In the past, several studies regarding the effect of small quantity addition of rare elements (RE) on the structural and mechanical characteristics of ODS alloys have been published [2, 3, 15-17]. The outcomes of these studies reveal that alloys composing of these elements exhibit higher mechanical performance and well-balanced uniform oxide particles compared with other traditional ODS alloys without containing these elements. Hoelzer et al. [18] were prepared 4 different samples comprising of 0, 0.25, and 0.3 Y_2O_3 wt% added 14Cr-ODS employing two diverse methods. They reported that the nanoparticles added alloys showed remarkably higher strength than oxide strengthened alloys for elevating temperatures. Meanwhile, the ductility performance of the oxide strengthened alloys was superior to that of the nanoparticles strengthened alloys. Xu et al. [19] found that the diverse annealing treatments was a crucial effect on the compositional fluctuations and design of nanoscale oxide dispersion performance. They reported that when annealing temperature reached to 1100 °C or above, the Ti enrich shell gradually vanished, and only Y-Zr rich oxide structures were stayed in structure. Various elements such as Hf, Ni, Ti and Zr added ODS steels have superior creep rupture strength than other ODS steels which does not include such elements [16, 20]. So, it is very important to clearly describe the microstructural and morphological changes of such minor elements during the mechanical alloying process, followed by the annealing or sintering parameters to be performed [3].

9Cr-ODS steel is an encouraging candidate material for nuclear energy powerhouses, a system that requires superior mechanic attitude at increased temperatures [21]. In particular powder metallurgy, the fabrication process has come across some challenges in obtaining precise composition control [22]. Some of the diffusing atoms, such as Cr, V, Nb, W, and Mo significantly influence mechanical properties. This is thought to happen by microstructural evolutions. Besides, the main contribution to the advanced mechanical and creep performance in comparison with other martensitic-based steels is assigned to the presence of the nanoscopic oxide precipitations in the matrix, which hinder the mobility of dislocations called as Orowan looping mechanism [23]. Hence, the mean interparticle distance between oxides in the matrix is one of the manipulating parameters that regulate the material system's microstructural changes and resultant mechanical properties. The solution limit of Y in Fe is also very poor at room temperature [24]. Thus, it is hard to solve Y into Fe matrix by conventional metallurgy process. Hence, ball

milling method is frequently chosen by various researchers to fabricate new Fe-based ODS steels [25, 26].

In this work, 9Cr prealloyed powders was selected matrix material and it was reinforced with Y_2O_3 0.5 wt% to produced ODS nanocomposite powders. The main purpose of this study was to examine size and structural changes of reinforcement phase (Y_2O_3) and the difference in the morphological structure and hardness properties of the mixed particles during ball milling and post-annealing treatment. This study exhibits recent improvements in the procedure of scrutinization of new generation 9Cr-ODS nanocomposite powders, to supply significant knowledge for microstructure control and hardness aspect in the context of structure-performance framework. In this regard, the combined influence of ball milling duration and annealing temperature on the microstructural evolution, particle size, crystal structures, and hardness properties of milled powders was assessed by using scanning electron microscopy (SEM), particle size analyzer and X-ray powder diffraction (XRD) analyses, energy-dispersive X-ray spectroscopy (EDX), and consequently hardness measurements.

2. Experimental Method

The prealloyed 9Cr ferritic powders consisting of Fe–9Cr–1Mo–1W–0.2V (wt%) composition plus nanosized ceramic powders of Y_2O_3 (0.5 wt%) (Nanografi, Turkey) was milled in a Retsch PM 200 high planetary ball milling device, utilizing 125 ml tungsten carbide (WC) jar and 7.5 mm WC balls maintaining a 15:1 ball to powder (BPR) weight ratio. The ball milling operation was performed under air atmosphere for 2, 8, and 16 hours employing rotation speed of 350 rpm with time interval i.e., milling operation was conducted 30 min and then rested 15 min till planned milling duration. The goal of such a milling procedure was to prevent increase high-temperature causing recrystallization in the plastically deformed powders. To eliminate severe cold welding and agglomeration, total amount of 2 wt% stearic acid was gradually added in milling system during each milling time was finished. Subsequently, 16 h milled powders were annealed at 700 °C, and 900 °C for 1 h in Protherm brand furnace. The particle size values and their distribution behavior after the milling was analyzed by particle size analyzer (Malvern Mastersizer 2000) using laser diffraction in wet distribution. The morphological alterations of the produced powders were monitored by scanning electron microscope (SEM, Zeiss Evo-LS10). Besides, an energy dispersive X-ray spectroscopy (EDX) module in the same SEM instrument was utilized to assess the chemical differences and dispersion behavior of the synthesized powders. A high-resolution X-ray powder diffractometer curves were collected by (Malvern Xpert³) XRD instrument to evaluate the differences in the phase composition and to identify phase formation for different

milling times.

According to available knowledge in the literature review [27, 28], the micro-Vickers hardness test was selected since it is suitable for multiphase structures due to its remarkably harder and smaller diamond indenter which minimize potential damage to the material during testing. The hardness test was performed with respect to different milling times in an ex-situ model. From each set powder group, a little amount of milled powders mounted in a 15 mm diameter bakelite and it left till fully cured. To calculate the hardness precisely, a smooth and homogenous sample surface is required. Thus, the bakelite molds were gently ground up to 2000 mesh fine SiC abrasive papers and ultimately, they polished to a reproduce finishing surface employing ultra-fine alumina paste (Ra: 0.25 μm). The micro-Vickers hardness measurement of each group was done utilizing a digital Innovatest W-HV400 Vickers-hardness tester under a constant load of 25 g and dwelling time of 15 s. To supply exactness and repeatability in the measurements, three identical samples were evaluated from each powder group. From each batch set, at least five different measurements were performed to insure accurate statistical sample and they were presented along with standard deviations and exemplary indentation figures. A schematic representation of the milling method and powder characterizations are illustrated in Figure 1.

3. Results and Discussions

3.1 Variation of Particle Shape and Size

Figure 2 exhibits the SEM images of initial 9Cr powders and 9Cr-ODS ferritic powders with respect to different milling times. Figure 3 shows the minimum ($d_{0.1}$), average

($d_{0.5}$), maximum ($d_{0.9}$) particle size of the milled powders. Considering both Figure 2 and 3, it was observed that the as-received (unmilled) powders showed irregular shape with an average particle size of 92 μm . It was seen that the 2h milled powders were slightly flattened, and the mean size of the particles was about 89 μm . The main reasons for such a little reduction were both the applied low milling time (2h) and the high effectiveness of the initial process control agent (stearic acid) on the milling systematics. After milling of 8h, the average size of the powders reached to maximum levels (100 μm) because the powders subjected to cold-welding and repetitive flattened mechanism and like as ‘corn-flakes structure’ was observed in the microstructure as shown in Figure 2. One reason for the observed particle shapes can be originated from shearing effect of hard WC milling balls on the 9Cr-ODS ferritic matrix powders. Such an inspections were commonly monitored by several researchers conducting a study on the mechanical alloying of similar systems [29, 30]. Further deformation up to 16h, the particle shape totally transformed into randomly fractured irregular shaped smaller pieces as shown in Figure 2. The average size of this powder system dramatically decreased to minimum level of 5 μm (See Figure 3) because of excessive work hardening and dominant fracture mechanism during the milling duration between 8h and 16h.

The monitored drastic reduction in powder size could also be assigned to the step by step fragmentation of thinned flakes (as indicated in Figure 4) into randomly fractured minor particles along with priorly existence of smaller irregular shaped powders. On the other hand, various researchers announced that the reduction in particle size was proof that fragmentation of flakes, creating new powder surface area [31].

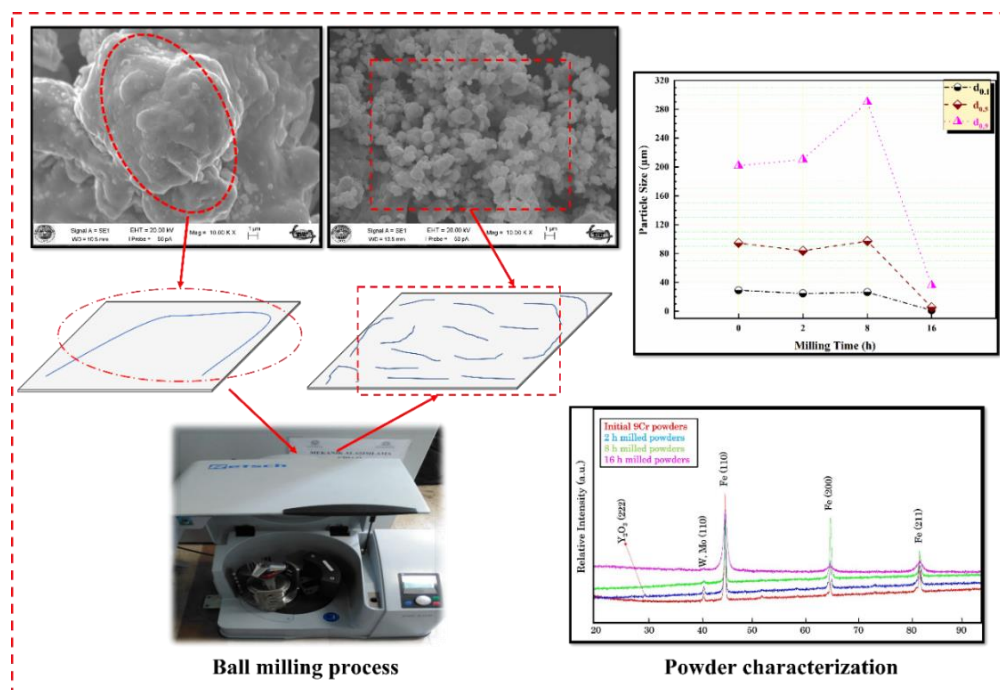


Figure 1. Schematic representation of ODS principle and milling operation, experimental setup and measurements

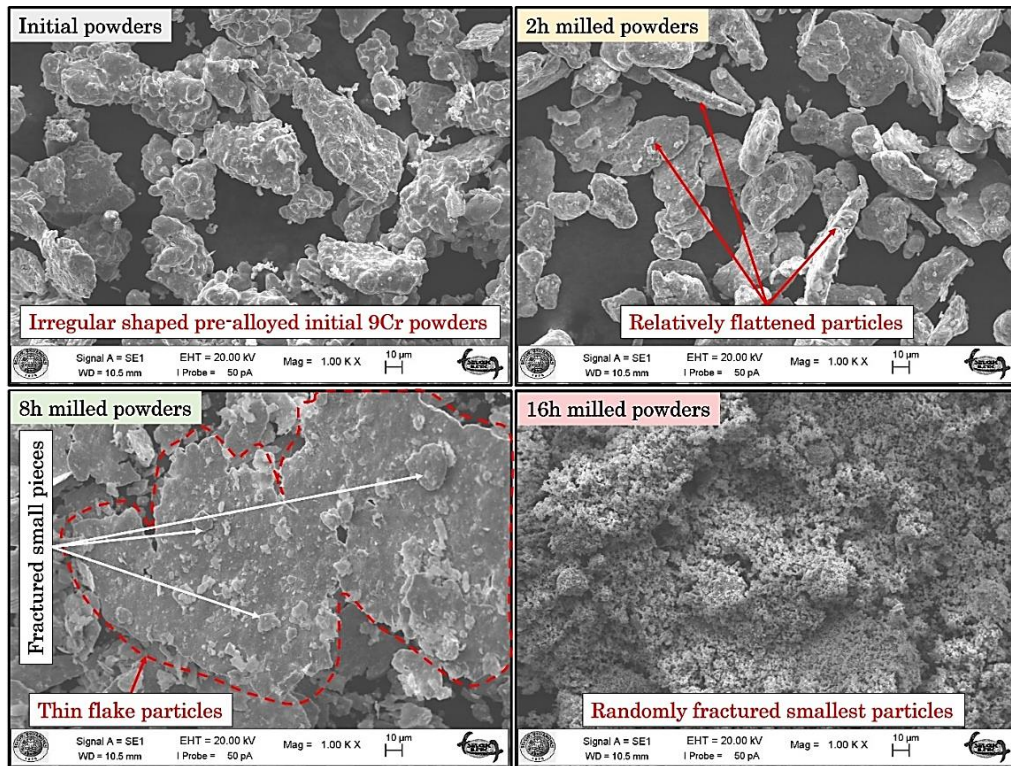


Figure 2. Particle shape changes of 9Cr unmilled powders and milled 9Cr-ODS powders at different milling times

The kind and quantity of process control agent (PCA) is one of the most important parameters affecting kinetics of mechanical alloying. Employing insufficient amount of PCA, the surface area of the powders covered by the PCA is restricted. In this case, overdone-cold welding is still going on and alloying is not given a chance. Nevertheless, if the sufficient amount of PCA can completely cover the surface area of the powders, the excess cold welding mechanism does not occur [32]. An equilibrium is fulfilled between cold welding and fracture mechanism, and alloying takes place instantly. As the increasing specific surface area, the effect of PCA has reached the desired level and alloying has occurred.

As shown in Figure 5, particle size distribution behavior of the initial powders displayed a homogeneous tendency. Since the low milling duration (2h) and effective PCA in the milling operation, a wide range of initial powders protected their initial shape and thus no discernible size distribution behavior was observed except for shifting towards lower angle due to reduced particle size. Plus, the particle morphology of the unmilled and 2h milled powders was nearly equiaxial as compared to further milling systems, as can be confirmed by examining Figure 2 and 5. However, this tendency gradually altered up to 16h milling duration. A broadened peak distribution towards to high particle size was achieved after 8h milled powders owing to numerous flake pieces resulted from rolling effect of milling medium. When

16h milled powders were examined, particle size distribution varied within a narrow range with bimodal distribution meaning it has two different peaks. Nevertheless, these peaks were monitored in the quietly low side of particle size. The reason for this is that the flake-structure powders were fractured with prolonged milling time and as a result of these fractures, the smallest particles were formed in all milling operation. This is a significant indication that the particle size powders are nonuniformly dispersed. In addition, as shown in the Figure 4, the cross sections of the powders reached about 800 nm due to the ball-wall, ball-ball and powder-powder collisions and this leads to easier breakage of the powders with random fragmentation resulting two diverse peaks in distribution behavior. After milling 16h, the mean particle size dramatically decreases from 101 μm to 5 μm , as shown in Figure 3. Considering particle size and morphology analyses, it can be assumed that the ball milling operation consist of two stages: cold-welding and fracture mechanism [33]. Firstly, initial powders experienced severe plastic deformation under the rolling effect of WC balls, and it led to flakes with very thin cross section, as depicted earlier in Figure 4. Secondly, such a thinned powders were effortlessly fragmented into minor sizes due to high impact of powder-powder, powder-jar, powder-ball crashes. As can be obviously experienced, ball milling process not only resulted in the shift of average size to lower values but also benefited the distribution tendency to narrow zone.

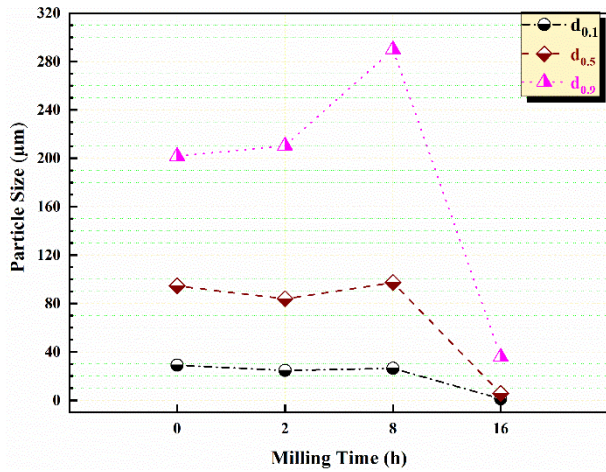


Figure 3. The differences in minimum, average, and maximum particle size for unmilled and milled powders with regard to increasing milling time

3.2 XRD and Crystal Structure Analyses

Figure 6 illustrates the XRD patterns of unmilled and milled powders. The monitored diffraction peaks belong to the Fe, Cr, W, Mo, and Y₂O₃ materials. However, no detectable diffraction peak was observed for V due to its quite low concentration (0.2 wt%) below the resolution limit of XRD instrument. As the increasing ball milling time, it was appeared that the peak intensity of Y₂O₃ vanished, which was assigned to its well distribution in the Fe matrix and accompanying reduction in particle size due to brittle solid behavior of hard ceramic Y₂O₃ phase. On the other hand, the diffraction intensities of Fe base metal and alloying elements decreased along with increased peak wideness except for 8h milled systems (to be explained in detail further). Considering available information in the classical theory of XRD, the widening reflection peak implies that the

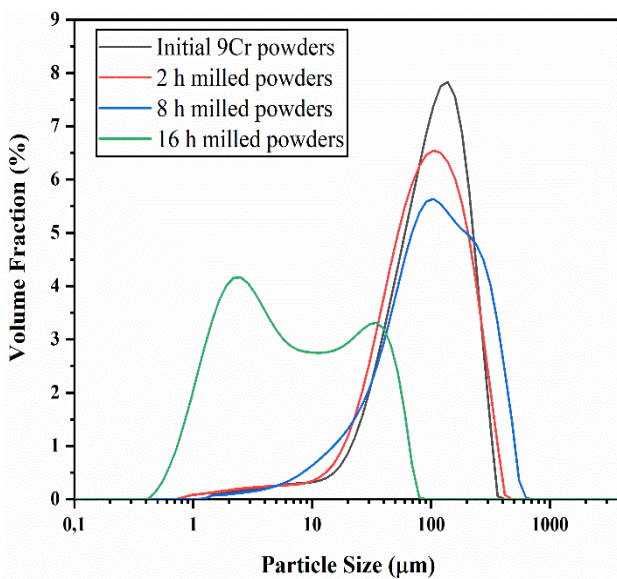


Figure 5. The variation on the particle size distribution behavior of powders in regard to milling duration

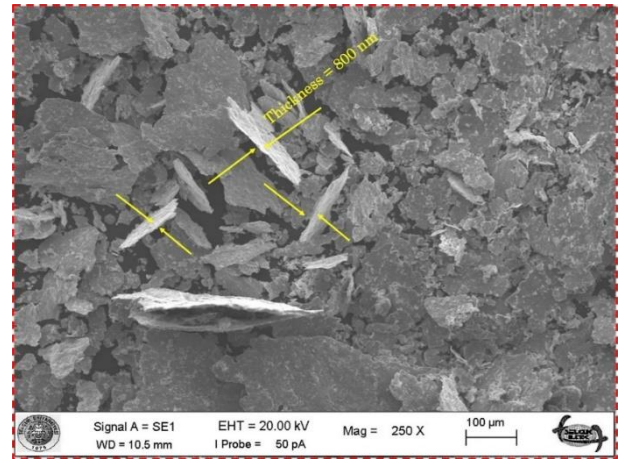


Figure 4. SEM image, indicating cross-section view of thinned flake 9Cr-ODS particles after 8h of milling

crystallite size or domain size reduces accompanying increasing lattice strain dependence on milling time [34]. At first glance, it was glittered that the (200) diffraction peak intensity of 8h milled powders (as described in green color) remarkably increased, and it also showed approximately same intensity in the main reflection of (110) direction. This observation perfected the particle shape image of illustrated in Figure 4, where flakes of 800 nm thickness were detected in 8h milled 9Cr-ODS powders. The detected texture formation was ascribed to the plastic deformation provoked by the thinned flake particles from the rolling effect of rigid milling medium [35]. Increasing milling time up to 16h resulted in vanishing of texture formation on the particles. The disappeared texture was related to the development of smaller particles because of the fragmentation of platelets or flakes after 16h of milling, as depicted prior in Figure 2.

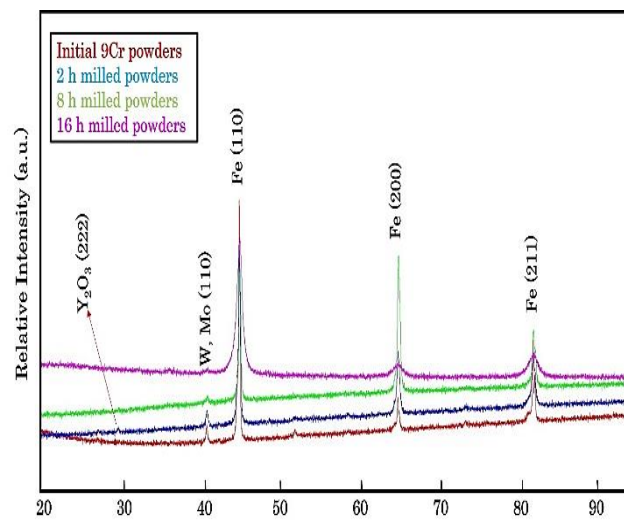


Figure 6. XRD diffraction patterns showing planes and phases of initial and milled powders at different milling duration

The crystallite (domain) size of the (110) and (200) diffraction curves of the produced powders evaluated by XRD data utilizing Scherrer equation [36] with respect to ball milling time is illustrated in Figure 7. As shown in Figure 7, increasing milling time resulted in reduction in crystallite size and concomitant widening of full width at half-maximum (FWHM) in the (110) reflection of Fe which is expected by virtue of ball milling and solid solution mechanism resulted by decreased crystallite size (D) with extended milling time. Severe and repeated collision of powders-ball-jar changed the crystallite size of main reflection (110) from 132.19 nm to 14.12 nm. Also, it could be inferred that prolonging milling time resulted in increment in both lattice distortion and dislocation numbers because dislocations, voids, interstitials, and other metallurgical defects led to intense plastic deformation during mechanical milling operation [37]. Hence, one observes that the mechanical alloying process not only improve the grain refinement of the powders but also augments both strain storage on the lattice and dislocation density. However, crystallite size increased up to 85 nm on (200) reflection which was attributed texture formation on this crystallographic direction, as described earlier in Figure 4 and 6. However, farther milling process created strict plastic deformation as a consequence high energy milling which was led to randomly arranged grain boundaries as barriers to dislocation movement and initiated solid-solution mechanism so, the domain size went down to 11.25 nm on (200) direction plane.

The micro-Vickers hardness of the 9Cr-ODS steel powders against different milling times is presented in Figure 8. The hardness of the powders improved from 160.74 Hv to 334.63 Hv with increasing milling time because of excessive plastic deformation of the powder particles. The synthesized powders exhibit excellent hardness properties than that of the traditional plastic deformation routes [38].

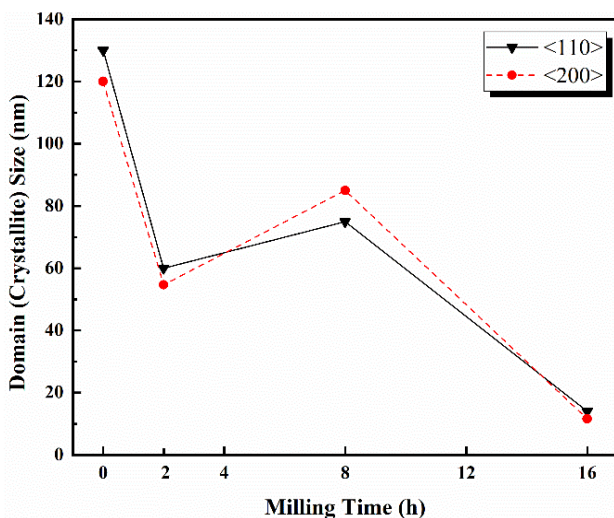


Figure 7. The alterations on the crystallite size of (110) and (200) plane direction of powders for different milling times

3.3 Hardness Properties of Milled Powders

These milled powders subjected to strain hardening owing to prolonged milling duration which results in an enhancement in hardness of the particles. Such an improvement on hardness of produced powders can be defined by several cooccurring factors. The grain refinement mechanism is the prominent one among them. Following Hall-Patch principle, which defines the correlation between hardness/strength of polycrystalline samples and the grain size, as the grain size decreases the hardness increases. This equation can be also utilized by different modified constants for nano-crystalline materials [39]. Another crucial factor is the increased stored energy on the lattice originating from the high dislocation density triggered by improving milling time. Moreover, different mechanisms such as dispersion, precipitation, and solid solution hardening/strengthening are also effective in increasing the hardness/strength of the powders [40].

3.4 Effect of Annealing Treatment on The Produced Powders

The high temperature development of the 16h milled powders can lead to precipitates, different phase transformations and grain growth mechanisms. To comprehend such an effect, XRD analysis was done on the annealed 16h milled powders. Figure 9 illustrates the XRD curves of as-milled (16h) and annealed powders at temperatures 700 °C and 900 °C. It was observed that all reflections exhibited a gradual decrement in FWHM meaning increment in crystallite size as a function of temperatures. The any intermetallic phases were not encountered in as-milled powders due to small amount of Y_2O_3 and strain triggered peak widening influence. The 700 °C annealed powders showed a Fe_3O_4 peaks. As for 900 °C, it was detected that Fe_2O_3 peaks in addition to Fe_3O_4 . These peaks were monitored earlier for different 9Cr-ODS powders, that increased milling time resulted in the aggregation of extra O in the material system and later these O react with the base Fe matrix to develop different Fe-O forms, which finally led to the development of Fe_2O_3 and Fe_3O_4 phases during elevating annealing temperature [41]. The present observations also showed good agreement with these studies. Moreover, the crystallite size of the main reflection of Fe was assessed utilizing Scherrer method, and chart describing the differences of crystallite size with respect to annealing temperature was illustrated in Figure 10. As the annealing temperature elevated, the crystallite increased to 67.25 nm and 160.53 nm for 700 and 900 °C, respectively. Figure 11 shows the hardness results with exemplary indentation of the annealed powders. The micro-Vickers hardness of the 16h milled powders slightly increased from 324.71 Hv to 325.35 Hv for 700 and 900 °C, respectively. It was observed that there were no clear changes among diverse annealing temperatures.

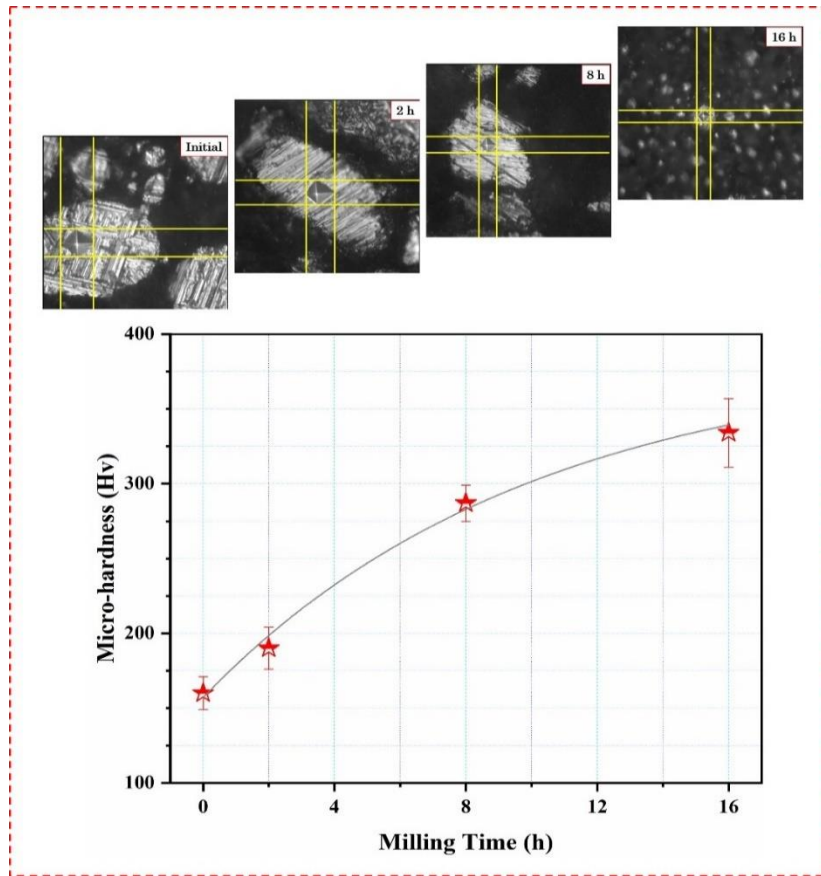


Figure 8. The micro-Vickers hardness changes of the milled powders with exemplary indentation images for different milling times

However, the annealed powders exhibited lower hardness as compared to as-milled powders, which was correlated with grain growth during elevating temperature, and it resulted in deteriorated hardness. On the other hand, oxide based intermetallic formation such Fe_2O_3 and Fe_3O_4 was beneficial for hardness due to their hard ceramic phases.

Concomitant influence of grain growth and formation of intermetallic, which were unfavorable and favorable impact on hardness resulted in such an indiscernible difference on hardness performance. One reason for this case could be originated from combined influences grain coarsening and

disappearing of structural defects inside of the powders due to thermal softening triggered by elevating annealing temperatures as reported by Nowik and Oksiuta [42].

To evaluate the aforementioned beneficial parameters on the hardness, SEM-EDS analysis was performed for 16h milled powders. The composition in the spectrum of 16h milled 9Cr-ODS powders employing EDX analysis showed in Figure 12. Figure represented atomic and weight percentage of content of distributed elements and their keV values.

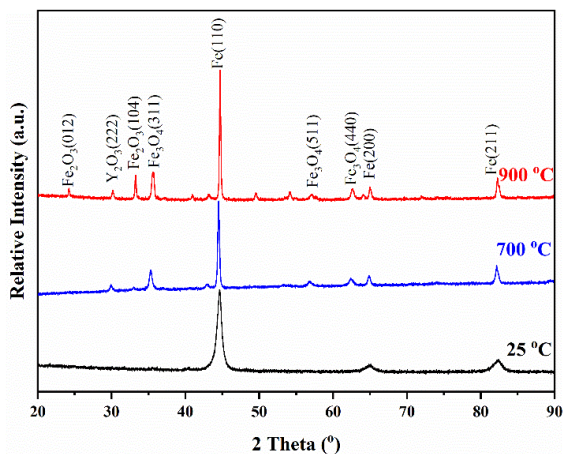


Figure 9. Crystallographical evolution of 16h milled 9Cr-ODS powders after annealing in ambient temperature, 700, and 900 °C

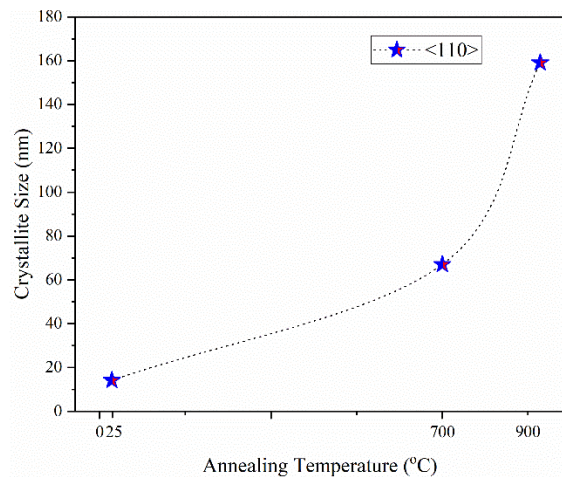


Figure 10. Dependence of crystallite size of 16h milled 9Cr-ODS powders for different annealing temperatures

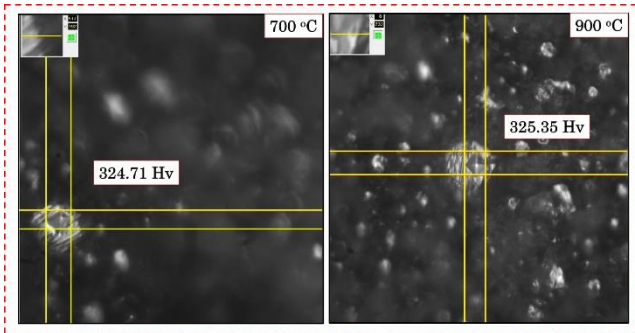


Figure 11. The micro-Vickers hardness and exemplary indentation images of annealed 16h milled nanocomposites powders

The constituent of dispersed elements was comprised of Fe, Cr, W, Mo, Y, O, and C, which were existent in the pre-alloyed and milled 9Cr-ODS powders. Even at small region, after 16h of milling protocol a well-balanced mixture of alloying elements was observed. As observed EDS analysis, alloying and reinforcement elements exhibiting uniform dispersion behavior throughout the matrix, may also lead to dispersion hardening mechanism.

To supply hypothesis about the uniform dispersion of hard ceramic Y_2O_3 phases and alloying elements EDX line analysis was also performed. As shown in Figure 13, the spectra of constituent elements of 16h milled 9Cr-ODS powders were detected with nearly same distribution behavior. Such an observations were proofed that followed milling protocol i.e., 16h of milling time was sufficient for uniform dispersion of alloying and reinforcement elements. These observations agreed with great extend to XRD and hardness results.

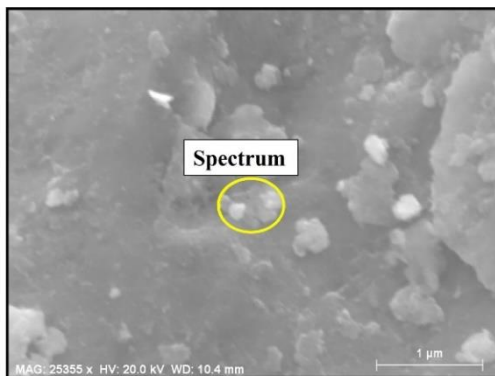


Figure 12. Results of the EDS analysis taken from indicated spectrum of 16h milled powders

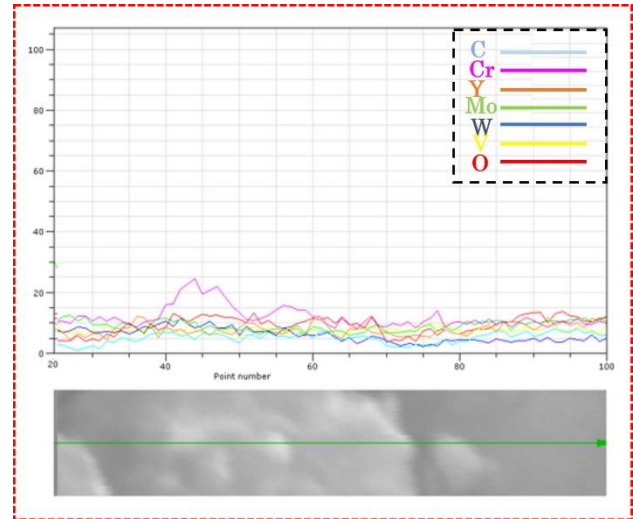


Figure 13. EDS line analysis of 9Cr-ODS powders milled for 16 h

4. Conclusions

In this paper, the 9Cr-ODS powders were synthesized by high planetary ball milling with different milling times (2, 8, and 16 h). The influences of milling duration on the microstructure, crystal structure and hardness properties of the produced powders were analyzed within the scope of structure-performance relationships. It was observed that the 16h milling protocol developed the minimum particle size (5 μm) as compared to initial form (92 μm) and these powders exhibited almost single phase (Fe) with solutioned alloying elements. Besides, it was observed that the strain hardening, Orowan precipitation and solid solution hardening mechanisms triggered by collisions of milling systematic constituents (powder, ball, and jar) were presumed to most dominant factors on the hardening properties. Such an effects led to an increment on the powder hardness 160 to 334 Hv for initial prealloyed 9Cr powders and 16h milled 9Cr-ODS powders, respectively. However, no discernible difference was observed as a result of the formation of beneficial intermetallic on the increase in hardness and the simultaneous occurrence of the harmful grain growth mechanism after annealing treatment of 16h milled powders. Based on observed outcomes, it could be concluded that despite increasing temperatures, the produced 9Cr-ODS nanocomposite powders did not compromised of its hardness and that the materials produced by the applied methods in here are a new alternative for high temperature applications.

Declaration

The author(s) declared no potential conflicts of interest with respect to the research, authorship, and/or publication of this article. The author(s) also declared that this article is original, was prepared in accordance with international publication and research ethics, and ethical committee permission or any special permission is not required.

Author Contributions

E. Salur is responsible for all sections of the paper

References

- McClintock, D.A., M.A. Sokolov, D.T. Hoelzer, and R.K. Nanstad, *Mechanical properties of irradiated ODS-EUROFER and nanocluster strengthened 14YWT*. Journal of Nuclear Materials, 2009. **392**(2): p. 353-359.
- Li, S., Z. Zhou, J. Jang, M. Wang, H. Hu, H. Sun, and L. Zhang, *The influence of Cr content on the mechanical properties of ODS ferritic steels*. Journal of Nuclear Materials, 2014. **455**(1-3): p. 194-200.
- Li, W., T. Hao, R. Gao, X. Wang, T. Zhang, Q. Fang, and C. Liu, *The effect of Zr, Ti addition on the particle size and microstructure evolution of yttria nanoparticle in ODS steel*. Powder Technology, 2017. **319**: p. 172-182.
- Chen, C.L. and Y.M. Dong, *Effect of mechanical alloying and consolidation process on microstructure and hardness of nanostructured Fe-Cr-Al ODS alloys*. Materials Science and Engineering: A, 2011. **528**(29-30): p. 8374-8380.
- Zinkle, S. and N. Ghoniem, *Operating temperature windows for fusion reactor structural materials*. Fusion Engineering and Design, 2000. **51**: p. 55-71.
- Clueh, R.L., J.P. Shingledecker, R.W. Swindeman, and D.T. Hoelzer, *Oxide dispersion-strengthened steels: A comparison of some commercial and experimental alloys*. Journal of Nuclear Materials, 2005. **341**(2-3): p. 103-114.
- Li, Z., Z. Lu, R. Xie, C. Lu, Y. Shi, and C. Liu, *Effects of Y₂O₃, La₂O₃ and CeO₂ additions on microstructure and mechanical properties of 14Cr-ODS ferrite alloys produced by spark plasma sintering*. Fusion Engineering and Design, 2017. **121**: p. 159-166.
- Chen, C., P. Wang, and G. Tatlock, *Phase transformations in yttrium-aluminium oxides in friction stir welded and recrystallised PM2000 alloys*. Materials at High Temperatures, 2009. **26**(3): p. 299-303.
- He, P., J. Hoffmann, and A. Möslang, *Effect of milling time and annealing temperature on nanoparticles evolution for 13.5% Cr ODS ferritic steel powders by joint application of XAFS and TEM*. Journal of Nuclear Materials, 2018. **501**: p. 381-387.
- Gökmese, H., B. Bostan, T.A. Yilmaz, and U. Tasci, *TEM characterization and synthesis of nanoparticle B₄C by high-energy milling*. International Advanced Researches and Engineering Journal, 2019. **3**(3): p. 195-201.
- Aktas, S. and E.A. Diler, *A review on the effects of micro-nano particle size and volume fraction on microstructure and mechanical properties of metal matrix composites manufactured via mechanical alloying*. International Advanced Researches and Engineering Journal, 2018. **2**(1): p. 68-74.
- Raghavendra, K.G., A. Dasgupta, P. Bhaskar, K. Jayasankar, C.N. Athreya, P. Panda, S. Saroja, V.S. Sarma, and R. Ramaseshan, *Synthesis and characterization of Fe-15 wt.% ZrO₂ nanocomposite powders by mechanical milling*. Powder Technology, 2016. **287**: p. 190-200.
- Hoffmann, J., M. Rieth, R. Lindau, M. Klimenkov, A. Möslang, and H.R.Z. Sandim, *Investigation on different oxides as candidates for nano-sized ODS particles in reduced-activation ferritic (RAF) steels*. Journal of Nuclear Materials, 2013. **442**(1-3): p. 444-448.
- Kotan, H., K.A. Darling, R.O. Scattergood, and C.C Koch, *Influence of Zr and nano-Y₂O₃ additions on thermal stability and improved hardness in mechanically alloyed Fe base ferritic alloys*. Journal of alloys and compounds, 2014. **615**: p. 1013-1018.
- Ukai, S., M. Harada, H. Okada, S. Nomura, S. Shikakura, K. Asabe, T. Nishida, and M. Fujiwara, *Alloying design of oxide dispersion strengthened ferritic steel for long life FBRs core materials*. Journal of Nuclear Materials, 1993. **204**: p. 65-73.
- Kimura, A., R. Kasada, N. Iwata, H. Kishimoto, C.H. Zhang, J. Isselin, P. Dou, J.H. Lee, N. Muthukumar, T. Okuda, M. Inoue, S. Ukai, S. Ohnuki, T. Fujisawa, and F. Abe, *Development of Al added high-Cr ODS steels for fuel cladding of next generation nuclear systems*. Journal of Nuclear Materials, 2011. **417**(1-3): p. 176-179.
- Isselin, J., R. Kasada, A. Kimura, T. Okuda, M. Inoue, S. Ukai, S. Ohnuki, T. Fujisawa, and F. Abe, *Effects of Zr addition on the microstructure of 14% Cr4% Al ODS ferritic steels*. Materials transactions, 2010. **51**(5): p. 1011-1015.
- Hoelzer, D. T., J. Bentley, M.A. Sokolov, M.K. Miller, G.R. Odette, and M.J. Alinger, *Influence of particle dispersions on the high-temperature strength of ferritic alloys*. Journal of Nuclear Materials, 2007. **367**: p. 166-172.
- Xu, H., Z. Lu, S. Ukai, N. Oono, and C. Liu, *Effects of annealing temperature on nanoscale particles in oxide dispersion strengthened Fe-15Cr alloy powders with Ti and Zr additions*. Journal of Alloys and Compounds, 2017. **693**: p. 177-187.
- Toloczko, M.B., D.S. Gelles, F.A. Garner, R.J. Kurtz, and K. Abe, *Irradiation creep and swelling from 400 to 600 C of the oxide dispersion strengthened ferritic alloy MA957*. Journal of nuclear materials, 2004. **329**: p. 352-355.
- Xu, Z., S. Liu, L. Song, X. Yang, Y. Zhao, and X. Mao, *Effect of silicon on oxidation behavior of 9Cr-ODS steel at 650° C*. Fusion Engineering and Design, 2021. **167**: p. 112384.
- Polat, G., A.B. Batibay, and H. Kotan, *Understanding microstructural evolution and hardness of nanostructured Fe89.5Ni8Zr2.5 alloy produced by mechanical alloying and pressureless sintering*. Engineering Science and Technology, an International Journal, 2020. **23**(5): p. 1279-1284.
- Xu, S., Z. Zhou, F. Long, H. Jia, N. Guo, Z. Yao, and M.R. Daymond, *Combination of back stress strengthening and Orowan strengthening in bimodal structured Fe-9Cr-Al ODS steel with high Al addition*. Materials Science and Engineering: A, 2019. **739**: p. 45-52.
- Kotan, H., *Effect of Y and nano Y₂O₃ additions on grain growth and hardness of nanocrystalline austenitic stainless steels produced by mechanical alloying*. Journal of the Faculty of Engineering and Architecture of Gazi University, 2019. **34**(3): p. 1266-1272.
- Kotan, H., *Thermal stability, phase transformation and hardness of mechanically alloyed nanocrystalline Fe-18Cr-8Ni stainless steel with Zr and Y₂O₃ additions*. Journal of Alloys and Compounds, 2018. **749**: p. 948-954.
- Darling, K.A., M. Kapoor, H. Kotan, B.C. Hornbuckle, S.D. Walck, G.B. Thompson, M.A. Tschopp, L.J. Kecskes, *Structure and mechanical properties of Fe-Ni-Zr oxide-dispersion-strengthened (ODS) alloys*. Journal of Nuclear Materials, 2015. **467**: p. 205-213.
- Mihalache, V. I. Mercioniu, A. Velea, P. Palade, *Effect of the process control agent in the ball-milled powders and SPS-consolidation temperature on the grain refinement, density and Vickers hardness of Fe14Cr ODS ferritic alloys*. Powder Technology, 2019. **347**: p. 103-113.

28. Sandim, H.R.Z., R.A. Renzetti, A.F. Padilha, D. Raabe, M. Klimenkov, R. Lindau, and A. Möslang, *Annealing behavior of ferritic–martensitic 9% Cr–ODS–Eurofer steel*. *Materials Science and Engineering: A*, 2010. **527**(15): p. 3602-3608.
29. Shi, W., L. Yu, C. Liu, Z. Ma, H. Li, Z. Wang, Y. Liu, Q. Gao, and H. Wang, *Evolution of Y_2O_3 precipitates in ODS-316 L steel during reactive-inspired ball-milling and spark plasma sintering processes*. *Powder Technology*, 2022. **398**: p. 117072.
30. Song, Q.S., Y. Zhang, Y.F. Wei, X.Y. Zhou, Y.F. Shen, Y.M. Zhou, and X.M. Feng, *Microstructure and mechanical performance of ODS superalloys manufactured by selective laser melting*. *Optics & Laser Technology*, 2021. **144**: p. 107423.
31. Salur, E., C. Nazik, M. Acarer, I. Savkliyildiz, and E.K. Akdogan, *Ultrahigh hardness in Y_2O_3 dispersed ferrous multicomponent nanocomposites*. *Materials Today Communications*, 2021. **28**: p. 102637.
32. Salur, E., M. Acarer, and İ. Şavkliyildiz, *Improving mechanical properties of nano-sized TiC particle reinforced AA7075 Al alloy composites produced by ball milling and hot pressing*. *Materials Today Communications*, 2021. **27**: p. 102202.
33. Salur, E., A. Aslan, M. Kuntoglu, and M. Acarer, *Effect of ball milling time on the structural characteristics and mechanical properties of nano-sized Y_2O_3 particle reinforced aluminum matrix composites produced by powder metallurgy route*. *Advanced Powder Technology*, 2021. **32**(10): p. 3826-3844.
34. Salur, E., *Synergistic effect of ball milling time and nano-sized Y_2O_3 addition on hardening of Cu-based nanocomposites*. *Archives of Civil and Mechanical Engineering*, 2022. **22**(2): p. 1-18.
35. Doğan, K., M.I. Ozgun, H. Subutay, E. Salur, Y.R. Eker, M. Kuntoglu, A. Aslan, M.K. Gupta, M. Acarer, *Dispersion mechanism-induced variations in microstructural and mechanical behavior of CNT-reinforced aluminum nanocomposites*. *Archives of Civil and Mechanical Engineering*, 2022. **22**(1): p. 1-17.
36. Patterson, A., *The Scherrer formula for X-ray particle size determination*. *Physical review*, 1939. **56**(10): p. 978.
37. Bicer, H., E.K. Akdogan, I. Savkliyildiz, C. Haines, Z. Zhong, and T. Tsakalakos, *Thermal expansion of nano-boron carbide under constant DC electric field: An in situ energy dispersive X-ray diffraction study using a synchrotron probe*. *Journal of Materials Research*, 2020. **35**(1): p. 90-97.
38. Albaaji, A.J., E.G. Castle, M.J. Reece, J.P. Hall, and S.L. Evans, *Effect of ball-milling time on mechanical and magnetic properties of carbon nanotube reinforced FeCo alloy composites*. *Materials & Design*, 2017. **122**: p. 296-306.
39. Xiong, H., Z. Li, X. Gan, L. Chai, and K. Zhou, *High-energy ball-milling combined with annealing of TiC powders and its influence on the microstructure and mechanical properties of the TiC-based cermets*. *Materials Science and Engineering: A*, 2017. **694**: p. 33-40.
40. Tekin, M., G. Polat, Y.E. Kalay, and H. Kotan, *Grain size stabilization of oxide dispersion strengthened CoCrFeNi- Y_2O_3 high entropy alloys synthesized by mechanical alloying*. *Journal of Alloys and Compounds*, 2021. **887**: p. 161363.
41. Ohtsuka, S., S. Ukai, M. Fujiwara, T. Kaito, and T. Narita, *Improvement of 9Cr-ODS martensitic steel properties by controlling excess oxygen and titanium contents*. *Journal of Nuclear Materials*, 2004. **329**: p. 372-376.
42. Nowik, K. and Z. Oksiuta, *Microstructure, Grain Growth and Hardness of Nanostructured Ferritic ODS Steel Powder during Annealing*. *Metallography, Microstructure, and Analysis*, 2021. **10**(3): p. 355-366.